ELSEVIER

Journal of Nuclear Materials 249 (1997) 17–32

journal of nuclear materials

Redistribution of the alloying elements during Zircaloy-2 oxidation

B. Cox *, H.I. Sheikh

Centre for Nuclear Engineering, University of Toronto, 184 College Street, Toronto, Ont., Canada M5S 3E4

Received 18 December 1996; accepted 30 May 1997

Abstract

The redistribution of the alloying elements from the intermetallic particles into the oxide matrix has been examined for oxides formed on Zircaloy-2 in steam at 400, 500 and 600°C. The outer area of the oxide where the alloying elements are fully oxidised was emphasised. At 400°C little migration of Fe, Cr or Ni for any distance greater than the particle radius away from the original particle boundary was found. Within one radius of this boundary only iron migrates out of the precipitate and forms local agglomerations of almost pure iron oxide around the particle periphery. After 500°C oxidation the iron has diffused to greater distances from the original particle boundary and segregates in individual ZrO_2 crystallites that are high in iron. Si is found segregated in the boundaries of such crystallites but not elsewhere. Chromium remains largely within the boundaries of the intermetallic but forms infrequent small 'growths' on the periphery. Small $Zr_2(Fe/Ni)$ particles show both iron and nickel diffusing out and segregating but this segregation happens within the particle boundary for $Zr_2(Fe/Ni)$ particles larger than 1 μm. At 600°C most of the alloying elements diffuse out of the particle volume into the oxide matrix, and little or no segregation outside the particle boundaries was found. These effects can be interpreted in terms of the local oxygen partial pressure within the oxide and the effect this may have on the diffusion of the alloying elements.
© 1997 Elsevier Science B.V.

1. Introduction

Of the alloying elements in the Zircaloys (Sn, Fe, Cr, Ni) only tin is in solid solution, and hence relatively uniformly distributed over the advancing oxide/metal interface during high temperature oxidation. Iron, chromium and nickel are essentially insoluble in the metal at low temperatures ($\leq$ 600°C) and are, therefore, present almost entirely in the form of second phase particles. There are two different intermetallic compounds present $Zr(Fe/Cr)_{2+x}$, which occurs in two structural forms, hexagonal (C14) and cubic (C15), and $Zr_2(Fe/Ni)$ with a tetragonal (C16) structure [1]. Both compounds occur in Zircaloy-2; only the Zr/Cr/Fe phase occurs in Zircaloy-4. The proportions of cubic and hexagonal $Zr(Fe/Cr)_{2+x}$ present can be varied by differing fabrication routes, but both are commonly present, usually with the hexagonal form predominant. The relative stabilities of the two forms may also be regulated by the presence of dissolved oxygen in them [2]. A small number of particles of other, insoluble impurities are also generally present [3].

During the initial oxidation of zirconium alloys a thin coherent oxide film of ZrO_2 forms over the whole surface, including any intermetallic particles lying in the surface [4]. The effective oxygen partial pressure for zirconium oxidation at the oxide/metal interface is very low, and the thermodynamics of the oxidation process [5] give an estimated value of this of 10^{-75} atm at 400°C. This is too low for Fe, Cr and Ni to oxidise at this point. Oxidation of these elements can only occur at some point between the oxide/metal and the oxide/environment interfaces at which the effective oxygen partial pressure for oxidation of these elements is reached (Fig. 1). The manner in which an intermetallic particle oxidises will therefore be determined by whether it was present in the original metal surface, or was subsurface at the start of oxidation.

* Corresponding author. Fax: +1-416 978 4155; e-mail: cox@ecf.toronto.edu

0022-3115/97/$17.00 © 1997 Elsevier Science B.V. All rights reserved.
PII S0022-3115(97)00191-8

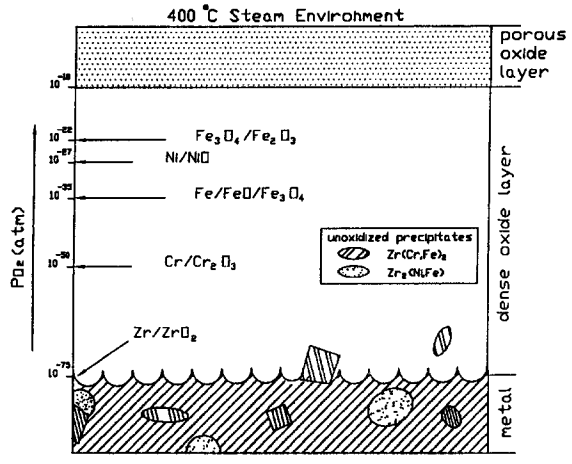

Fig. 1. Schematic diagram of the oxide film formed on Zircaloy-2 in 400°C steam illustrating the pO_2 values for Zr, Cr, Fe and Ni oxidation in the oxide film and some unoxidised precipitates.

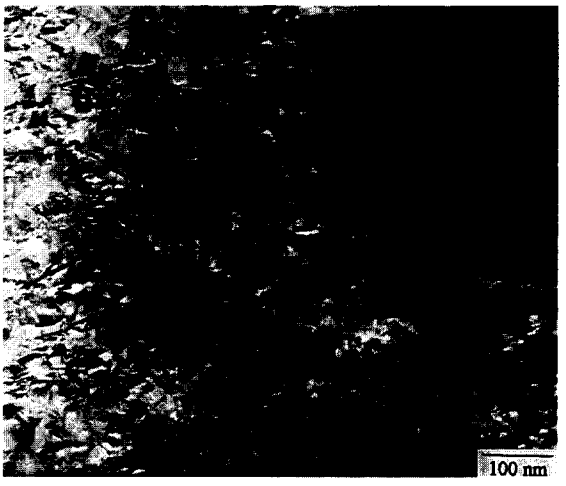

Fig. 3. Bright-field TEM micrograph of ZrO_2 crystallites at the 400°C oxide surface.

The behaviour of intermetallic particles in the original metal surface (or whose distance below it was very small compared to their diameters) has been considered earlier [4,6,7]. In this instance a thin coherent ZrO_2 layer is formed first, and the Fe and Cr then diffuse through this to the environmental interface where they form oxides of iron (Fe_3O_4, Fe_2O_3) and chromium (Cr_2O_3) respectively [6–8]. The manner in which they diffuse to the surface is not known at present, but there is some evidence [7] that Fe may remain unoxidised during this process.

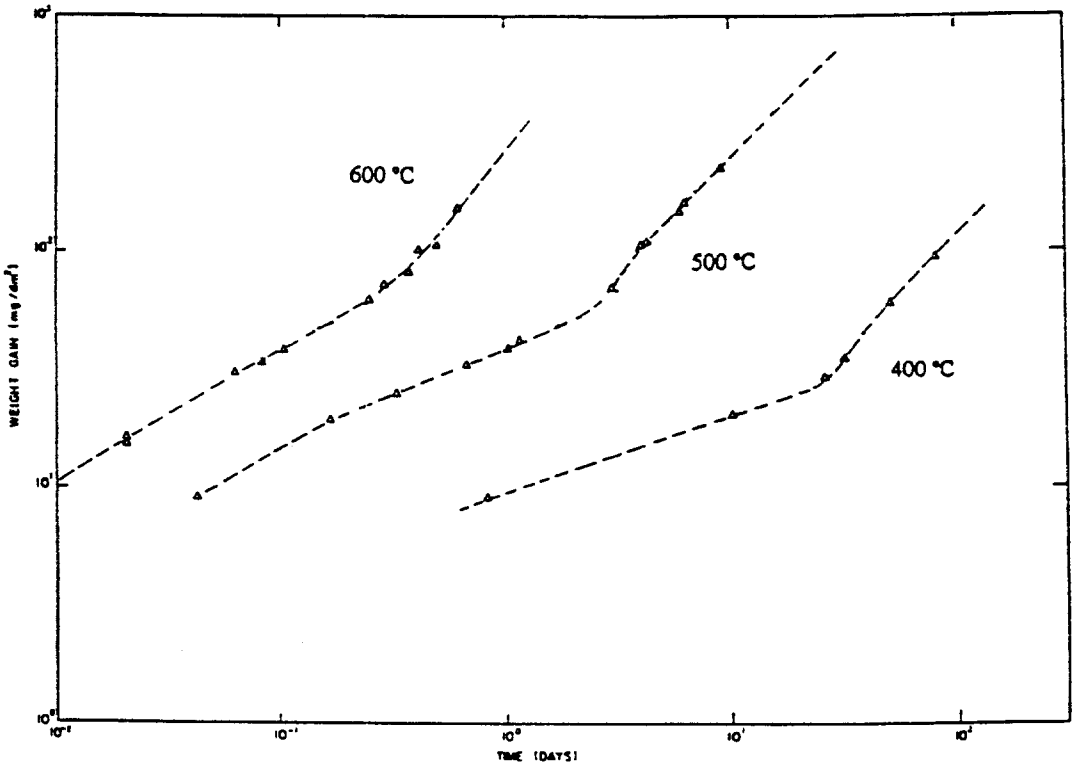

Fig. 2. Corrosion curves for Zircaloy-2 in atmospheric pressure steam at 400, 500 and 600°C [14].

The sequence of events that occurs for intermetallics that are initially more deeply buried in the metal is more complicated. It has been observed [9] that the $Zr(Fe/Cr)_{2+x}$ particles do not start to oxidise immediately after the oxide/metal interface passes them, but remain metallic until they are 100–200 nm away from this interface. While they are still electrically connected to the metal the intermetallics are cathodic to the matrix, and are thus cathodically protected from oxidation [10]. It has been found that the layers of oxide close to the metal/oxide interface are highly conducting, and appear as simple resistances during AC impedance spectroscopy [11]. Hence, although initially the embedded intermetallics are completely surrounded by the oxide matrix, this oxide may be so electrically conducting that they still maintain electrical contact with the metal and continue to be cathodically protected. When this cathodic protection is lost the Zr component of the intermetallic particle rapidly oxidises, and the Fe is rejected and appears as bcc Fe particles within the original boundaries of the particle. Precisely what happens then is not clear. There is evidence that Fe migrates out of the original particle volume, but little is definitely known about how it does this, or where it ends up. The local effective oxygen partial pressure is still too low to allow iron to oxidise to the Fe^{2+} or Fe^{3+} condition, but some interaction of oxygen with the bcc Fe particles may start at this point.

The aim of this study was to try to locate the Fe, Cr and Ni after $Zr(Fe/Cr)_{2+x}$ and $Zr_2(Fe/Ni)$ intermetallic particles have become completely oxidised, and especially to try to establish whether these species occupy positions in the bulk of the oxide crystallites, or are preferentially located in the crystallite boundaries. The behaviour of impurity atoms, such as Si, which are often present in the $Zr(Fe/Cr)_{2+x}$ and $Zr_2(Fe/Ni)$ phases (although they may also be present as separate silicide or silicide/phosphide particles) was also pursued, since this may be relevant to the nucleation of the nodules during nodular corrosion [12,13].

2. Experimental

The specimens for investigation were selected from a set of samples of Zircaloy-2 (batch Ac), that had been

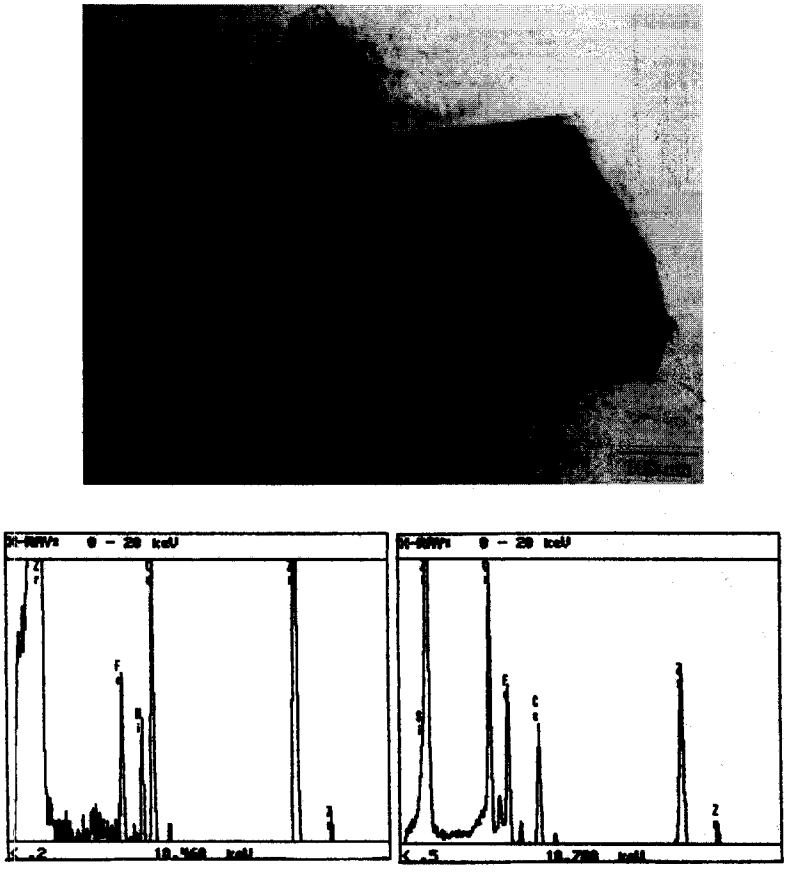

Fig. 4. Bright-field TEM image of an unoxidised $Zr_2(Ni, Fe)/Zr(Cr, Fe)_2$ intermetallic particle pair together with their EDX spectra.

Table 1

Test conditions	Weight gain (mg/dm^{-2})	Oxide thickness (μm)	Appearance
Zircaloy-2 sample details			
400°C steam/984 h	49	3.3	black uniform
500°C steam/151 h	161	10.7	black uniform
600°C steam/10 h	101	6.7	black uniform
Unoxidised	–	–	–

Analysis of Zircaloy-2

Element	Zr	Fe	Cr	Ni	Sn
wt%	bal.	0.145	0.1	0.055	1.47

oxidised in steam at 1 atm pressure at either 400, 500 or 600°C [14]. The selected samples were from positions on the corrosion curves just after the kinetic transition, at positions where the posttransition porosity would just be developing in the oxide (Fig. 2). The details of the specimens selected are given in Table 1. By choosing specimens oxidised in low pressure steam it was expected that processes that might have dissolved some components of

Fig. 5. A bright-field image of an hcp-type $(Cr, Fe)_2$ precipitate, its EDX spectrum and the SAD pattern acquired from the precipitate.

the oxide in aqueous solution [15] or where material might be volatile in high-pressure steam [12] would not be operating.

The samples were initially cut to prepare cross-sectional thin sections for transmission electron microscopy (TEM) [16]. However, the ion-mill available was unable to uniformly thin both the ZrO_2 film and the Zr metal matrix. Oxide bridges were always left that were too thick for TEM imaging, and broke if further attempts were made to mill them to transparency. In order to get specimens of oxide thin enough for TEM, therefore, the oxide was stripped and thinned by the technique described by Airey and Sabol [17], with some minor modifications. Oxides were ion-milled from either the metal or the oxide sides and sometimes from both sides.

Preliminary examination of the thinned oxide sections and mapping of the locations of interesting intermetallics was performed on the Philips EM430 at Mount Sinai Hospital. The sections were then transferred to the JEOL-2010F, equipped with a LINK-ISIS analytical system at McMaster University. This was initially operating with a probe size of ~ 1.0 nm and a maximum magnification of 800k × in STEM mode. However, it was upgraded to operate with a 0.5 nm probe and 1000k × magnification during the course of this study. This upgrade improved the ability to view and analyse crystallite boundaries in oxides where crystallite sizes were often only 10–20 nm in cross-section.

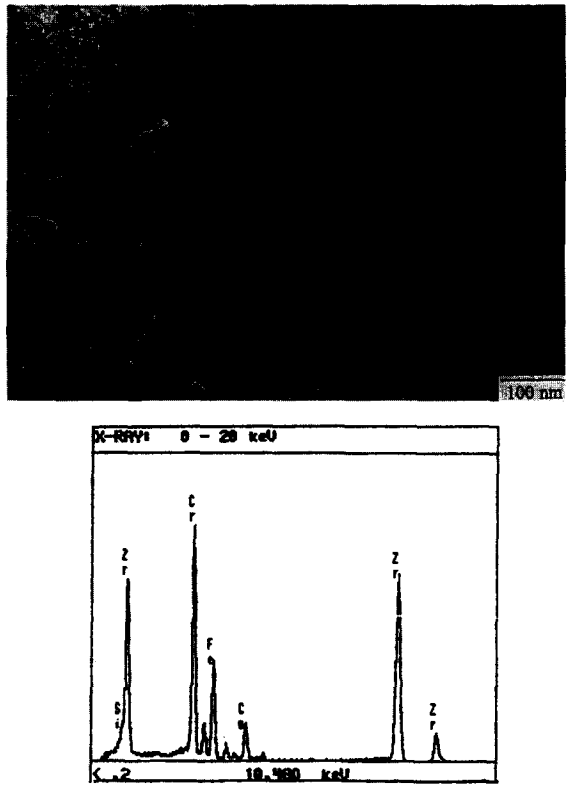

Fig. 6. Bright-field TEM image of an oxidised $Zr(Cr, Fe)_2$ precipitate at the 400°C oxide surface and its EDX spectrum.

3. Results

The oxide crystallite structure, for a specimen oxidised at 400°C, and well away from any intermetallic particles is shown in Fig. 3. The cross-sections of the crystallites, which were probably columnar [18] are irregular, show Moiré fringes as a result of overlapping and are relatively large (30–40 nm). Fe and Cr contents measured by EDX analysis were barely above background. Intermetallic particles within ~ 100 nm of the oxide-metal interface were still metallic, as reported previously [9]. Fig. 4 shows a pair of intermetallics where the $Zr(Fe/Cr)_{2+x}$ particle (right) has nucleated on the $Zr_2(Fe/Ni)$ particle (left) that precipitates first during cooling from the β-phase, where all alloying elements are in solution. Note that the Fe/Ni ratio in the left hand particle is > 1, which is typical of these particles, whether isolated or paired with a $Zr(Fe/Cr)_{2+x}$ particle. The Fe/Cr ratio of the $Zr(Fe/Cr)_{2+x}$ particle in this pair is, however, much less than one, and considerably less than the value of 0.8–0.9 typical of an isolated $Zr(Fe/Cr)_{2+x}$ particle in this batch of material (Fig. 5). This reduction of the Fe/Cr ratio in $Zr(Fe/Cr)_{2+x}$ particles nucleating on a previously formed $Zr_2(Fe/Ni)$ particle was typical of such pairs of particles.

After exposure at 400°C the oxidised intermetallics near to the oxide/environment interface showed irregular boundaries which appeared to consist of a series of 'growths' or pustules on the particle surface (Fig. 6). The iron to chromium ratio of these particles was lower than for the initial unoxidised particles. X-ray maps of such a particle showed that the 'growths' on the particle surface were high in iron and oxygen, whereas chromium remained almost completely within the initial boundaries of the precipitate (Fig. 7). Si was segregated within the particle and in an area adjacent to one of the iron oxide 'growths'. Spot analysis scans across three of the 'growths' on this particle (Fig. 8) showed that the growths were almost pure iron oxide, with very little chromium and only about 8 at.% Zr. The results from profile #1 are shown in Fig. 9. These 'growths' were quite typical of the fully oxidised intermetallics, although they were not always as widely distributed around the periphery of the particle as in the first example (above). They were often difficult to see in the imaging conditions in the Philips TEM, but were more easily visible in STEM mode in the JEOL-2010F. A second example of these 'growths' is shown in the TEM in Fig. 10, and the X-ray maps obtained in STEM mode are shown in Fig. 11. This was initially thought to be a $Zr_2(Fe/Ni)/Zr(Fe/Cr)_2$ pair, but no evidence of Ni could be found in either particle, and it was concluded that the

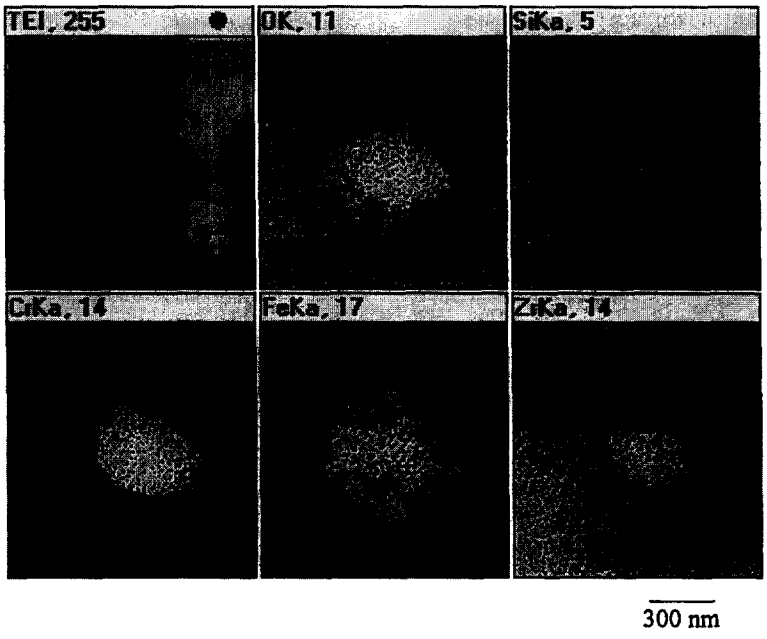

Fig. 7. X-ray maps acquired in STEM mode of the precipitate shown in Fig. 6.

'second particle' was actually a very large iron oxide 'growth' that had almost completely depleted the initial $Zr(Fe/Cr)_2$ particle of iron. Some other small iron oxide growths were, however, still formed around the particle periphery, inside which most of the chromium remained. Spot analysis scans again confirmed the very low Cr level in the iron oxide 'growth' and the presence of 6–10 at.% Zr in different areas.

After oxidation at 500°C evidence of these very localised iron oxide 'growths' was found infrequently, and they were not as distinct (Figs. 12 and 13). Iron contents in the oxide matrix adjacent to the particles (Fig. 12-oxide matrix analysis) were much higher than were observed at

Fig. 8. STEM image of the same precipitate showing the locations of the X-ray analysis profiles that were measured. Each profile consisted of 20 spot analyses at equal intervals along the line indicated. The measurements stopped after spot 7 of profile 3.

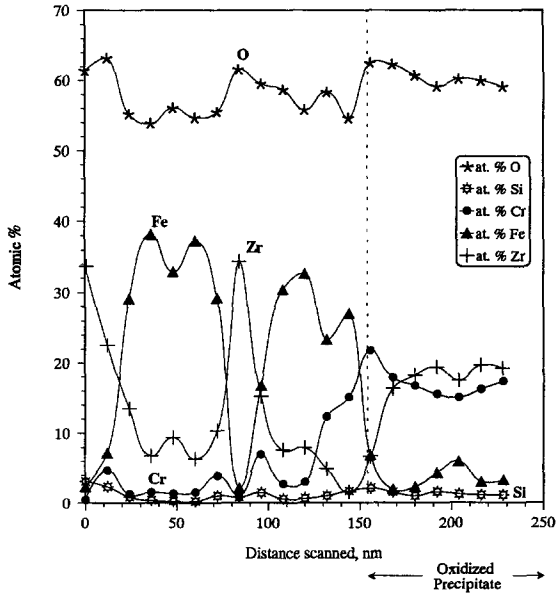

Fig. 9. X-ray analysis profiles for line #1 of the image in Fig. 8.

400°C. The X-ray maps showed that some evidence for chromium migration out of the particles, with segregation as small 'growths' on the particle periphery was now evident (Fig. 13). In $Zr_2(Fe/Ni)$ particles diffusion out of the particle appeared to be more restricted than diffusion out of $Zr(Fe/Cr)_2$ particles. For small $Zr_2(Fe/Ni)$ particles both Fe and Ni appear to diffuse out and segregate as mixed oxides. The same was not the case for large particles (> 1 μm). A very large oxidised $Zr_2(Fe/Ni)$ particle with a small $Zr(Fe/Cr)_2$ particle growing on it is seen in Figs. 14 and 15. The iron and nickel content has segregated as small mixed iron/nickel oxide particles within the original boundaries of the intermetallic, although both an iron and a nickel diffusion profile away from the particle appear to be present. Details of some of these segregated oxide particles are given in Figs. 16 and 17. All these oxide particles contain both Fe and Ni. A single small segregated Cr oxide particle appears to be present (right lower edge of Fig. 17) and may be associated with iron, but not nickel.

Oxide crystallite sizes in oxidised intermetallics and segregated iron and nickel oxides are very small and not easily studied individually. However, in the iron diffusion zone outside an intermetallic oxidised at 500°C, the crystallite size soon returns to that typical of the oxide matrix (i.e., 10–40 nm). Examination of the iron distribution in

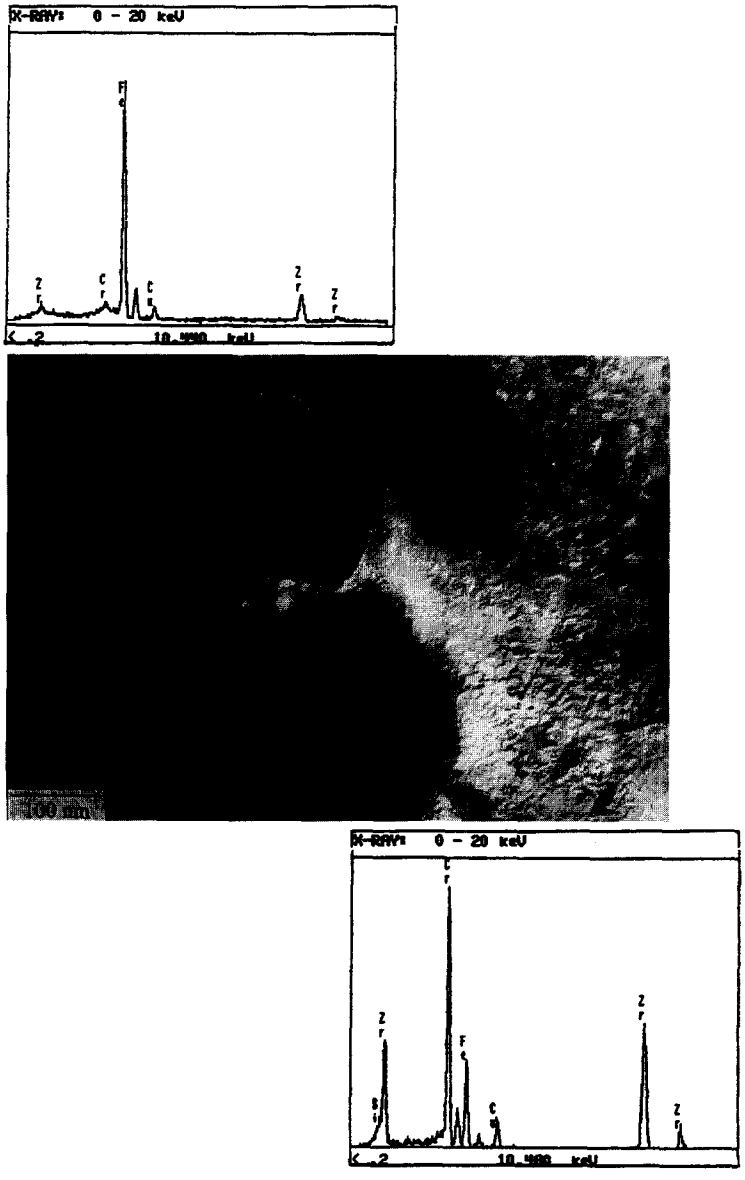

Fig. 10. Iron oxide growth and oxidised $Zr(Cr, Fe)_2$ precipitate in oxide formed at 400°C, together with their EDX spectra.

such a region shows that at the periphery of the iron diffusion profile away from the original intermetallic volume (Fig. 18) the iron segregates in individual oxide crystallites. These are seen in more detail in Fig. 19, where the Moiré fringes at the top show that there are overlapping crystallites. Thus, it cannot be concluded that any apparent crystallite boundaries are either normal to the foil surface or pass right through the foil. Line scans across the high iron crystallite at the top left of Fig. 19, avoiding the area showing Moiré fringes (Fig. 20), were made for each of the elements of interest (Fig. 21) and show that the iron is concentrated within the crystallite, which shows a shallow dip in Zr concentration. Rough estimates of the maximum Fe, minimum Zr and average O concentrations give ~ 15, ~ 25 and ~ 60 at.%, respectively. It is interesting that a minor segregation of Si (~ 5 at.%) occurs at the boundaries of the high iron crystallite, and that the breadth of the Si peaks suggests that the crystallite boundaries were not normal to the foil surface. No Si segregation has been found at crystallite boundaries that did not contain high iron concentrations. This localisation of iron well away from a precipitate was seen only after oxidation at 500°C.

In oxides formed in steam at 600°C the location of the intermetallics in the oxide was much more difficult as the boundaries of the initial precipitate became indistinct, and much of the Fe, Cr or Ni content had diffused out. The appearance of a $Zr_2(Fe/Ni)$ precipitate in TEM mode is shown in Fig. 22. This precipitate was found again in the JEOL-2010F for detailed X-ray mapping (Fig. 23) but revealed little segregation of the Fe and Ni. The original precipitate was depleted in both Fe and Ni, but only Ni showed evidence of some minor segregation at the precipitate periphery. The remains of a $Zr(Fe/Cr)_2$ precipitate (much of which had been ion-milled away as it was at the edge of the perforation of the foil) is seen in Fig. 24. It showed that much of the chromium was still present in the precipitate area, whereas the iron was almost uniformly distributed in the oxide matrix with little remaining segregated in the precipitate (Fig. 25). In this instance large oxide crystallites were formed right up to the precipitate boundary but a high resolution X-ray map of this area showed no evidence of iron segregating in individual crystallites as was observed at 500°C. X-ray spot analysis scans across this precipitate matrix boundary showed chromium peaking at ~ 18 at.% at the particle periphery, with iron at a maximum of 5 at.%, Zr at 30–35 at.% and oxygen at 50–55 at.%. Thus, although chromium shows a sharp boundary at the periphery of the original particle, diffusion of both Fe and Cr out of the particle has occurred since their total percentage is always less than that of Zr, while initial atomic percentages of Fe + Cr were close to twice that of zirconium.

4. Discussion

The initial stages in the oxidation of intermetallics in the Zircaloys, where the zirconium is oxidised and the iron is rejected to form bcc particles, within the volume of the

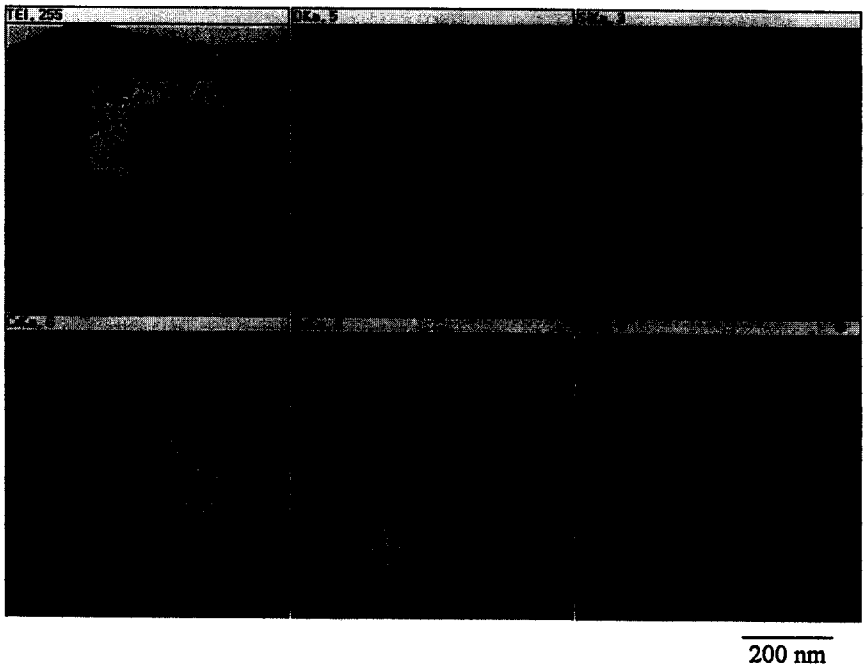

Fig. 11. X-ray maps acquired in STEM mode of the iron oxide particle and the oxidised intermetallic seen in Fig. 10.

original particle, have been reported [9]. The later stages, where the iron becomes oxidised are not so well understood. The diffusion of iron out of the particle volume has been observed [19–21], but the measurements have only looked at the average distribution of iron in the diffusion zone, and have not attempted to establish the location of the iron on a nanometric scale. Results obtained here show that iron, that was probably segregated initially as bcc Fe within the particle boundary, starts to migrate out of this region as the local pO_2 increases, but at 400°C diffusion is slow enough that it cannot migrate far, and segregates as agglomerates of iron oxide (Figs. 6 and 7). These may be scattered roughly uniformly around the original particle periphery, or may occur as only one major, and a few minor, agglomerates (Figs. 10 and 11). These agglomerates appear to be detached from the particle boundary as compositional scans show Zr increasing, and Fe and Cr decreasing briefly at or near the original particle boundary (Fig. 9) and between agglomerates.

After oxidation at 500°C, the occurrence of iron oxide agglomerates was infrequent, a more regular and extensive diffusion of iron out of the intermetallic occurred, and this diffusion profile became very localised near its limits (Figs. 18 and 19). This localisation consisted of individual oxide crystallites that were high in iron (up to ~ 15 at.%) but still appeared to be basically ZrO_2 (Figs. 20 and 21) with ~ 25 at.% Zr and ~ 60 at.% O. The localisation of Si at the boundaries only of these high Fe crystallites suggests that iron may be migrating in association with Si in this instance. Si concentrations in and at the boundaries of the agglomerates of iron oxide formed at 400°C were not found, although occasional indications of Si segregation were observed (Fig. 7, top of particle). At this time, however, the resolution of the microscope had not been upgraded, and this coupled with an error in locating profile #3 (Fig. 8) resulted in no clearer evidence of this segregation being obtained. There is little evidence on which to base expectations of the behaviour of SiO_2 in ZrO_2. In work on additions of small amounts of SiO_2 to stabilised ZrO_2 [22] the presence of 5% SiO_2 resulted in superplastic behaviour as a result of the formation of a thin (1 nm) amorphous grain boundary SiO_2 phase. It is possible that

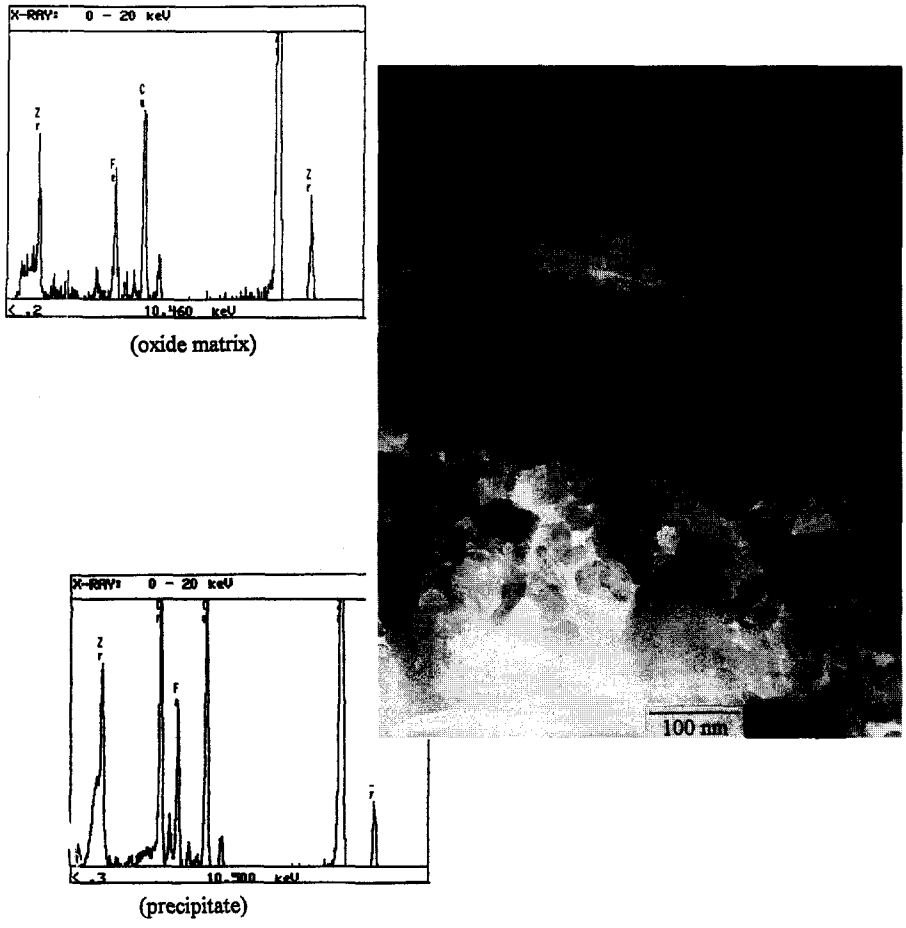

Fig. 12. Oxidized $Zr(Cr, Fe)_2$ precipitate and the EDX spectra from the oxide matrix and the precipitate after oxidation at 500°C.

the formation of an even thinner crystallite boundary phase on the high Fe crystallites could account for the observations here. The chromium still remains relatively immobile in oxides formed at 500°C, although some small Cr oxide growths were observed on the periphery of some intermetallic particles.

Oxides formed at 600°C showed much diffusion of both Fe and Cr out of the intermetallics. While there was only a minor remaining concentration of iron at the original precipitate site, there was about 15 at.% Cr remaining, still with a sharp concentration change at the original precipitate boundary. Unlike the situation at 500°C, where the very small (< 10 nm) crystallite size inside the original precipitate volume only changed back to a more normal 20–40 nm crystallite size at about the end of the iron diffusion profile, at 600°C large oxide crystallites were present right at the prior particle boundary. Since the iron appeared to be almost uniformly distributed outside the particle boundary at a concentration that must be somewhat less than the average iron content of the alloy (0.2 at.%), as there is still some concentration of Fe remaining in the precipitate volume, it is tempting to relate the small crystallite size in the particles to an effect of iron. We do not know at present whether the crystallites within the original particle volume comprise a mixture of very small ZrO_2 and Cr_2O_3 [8] crystallites or to a solid solution of the two. It has been impossible so far to resolve individual crystallites in such regions as there always appear to be multiple overlapping crystallites that prevent a distinction being made. With the new improved resolution of the JEOL-2010F there is some hope that an answer to this question may be possible in the future.

The key to the oxidation behaviour of the Zircaloys may lie in the behaviour of the Fe. Near to the oxide/metal interface the Fe is rejected and forms bcc iron particles within the particles. Fe does not appear to be mobile under these very low pO_2 conditions. What might cause it to begin to migrate out of this area as the local pO_2 increases? There is little helpful information in the literature, but two very diverse pieces of work may provide some clues. In the first [23], a study was made of the wetting of ZrO_2 furnace linings by molten iron. It was observed that when the iron was very pure and low in oxygen it did not wet the ZrO_2. However, as the iron progressively absorbed oxygen it began to wet the ZrO_2 and ultimately diffused rapidly along the ZrO_2 grain boundaries. If we can draw an analogy with the rejected iron particles, then, as the local pO_2 increases a point will be reached where oxygen will start to dissolve in them. This may be enough to start the outward diffusion of the iron. However, at this point the iron will still be metallic, although there may be an Fe–O binding energy that enhances the diffusion. We have no evidence for it migrating along the ZrO_2 crystallite boundaries in this case.

Once the iron becomes oxidised at a local $pO_2 \geq 10^{-35}$ atm (at 400°C) we need to know whether it can continue to diffuse into the ZrO_2. Here the second group of studies [24–26] may be important. In this series of papers, all

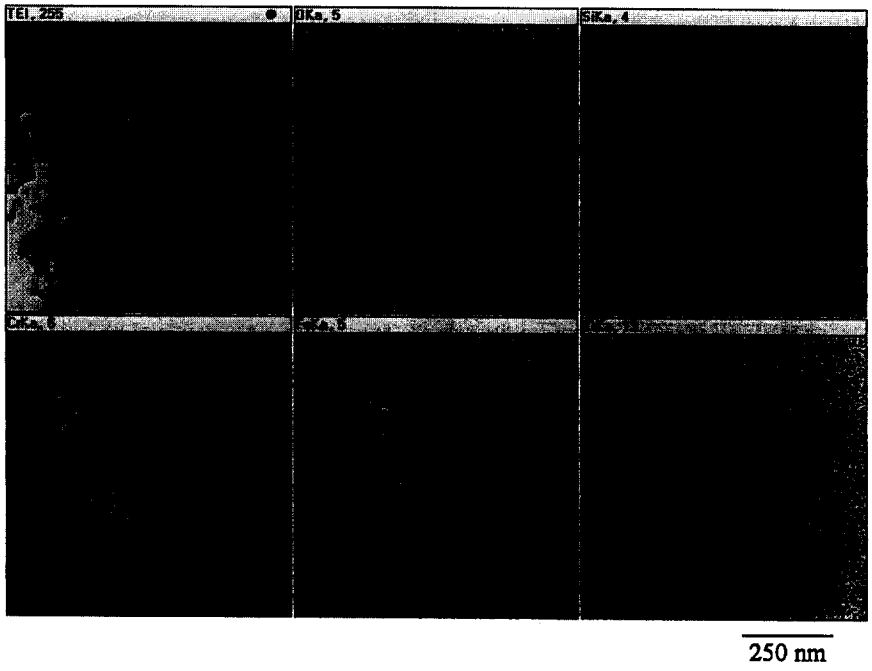

Fig. 13. X-ray maps acquired in STEM mode from the precipitate seen in Fig. 12.

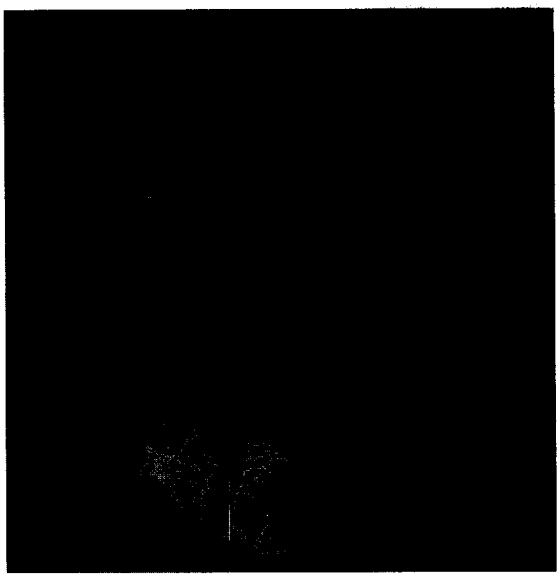

Fig. 14. STEM image of many small iron/nickel oxide particles probably from a large oxidised Zr_2 (Ni, Fe) particle.

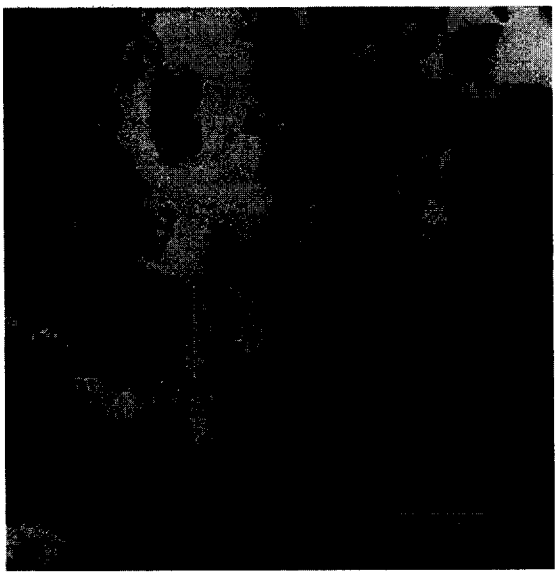

Fig. 16. High magnification STEM image of the area indicated by the window in Fig. 14.

based on ceramic studies at high temperature, we find evidence that Fe^{3+} (undersized) migrates rapidly in ZrO_2 containing oversized dopants as a result of a binding energy to oxygen vacancies [24]. Perhaps in the Zircaloys the tin provides the oversized dopant and, as it will also be in a valence state less than four throughout most of the thickness of the impervious oxide, perhaps it also affects the local oxygen vacancy content. Tin is one of the few alloying elements observed to increase the cubic rate constant during pretransition oxidation at high temperatures

Fig. 15. X-ray maps acquired in STEM mode from the oxidised particles seen in Fig. 14.

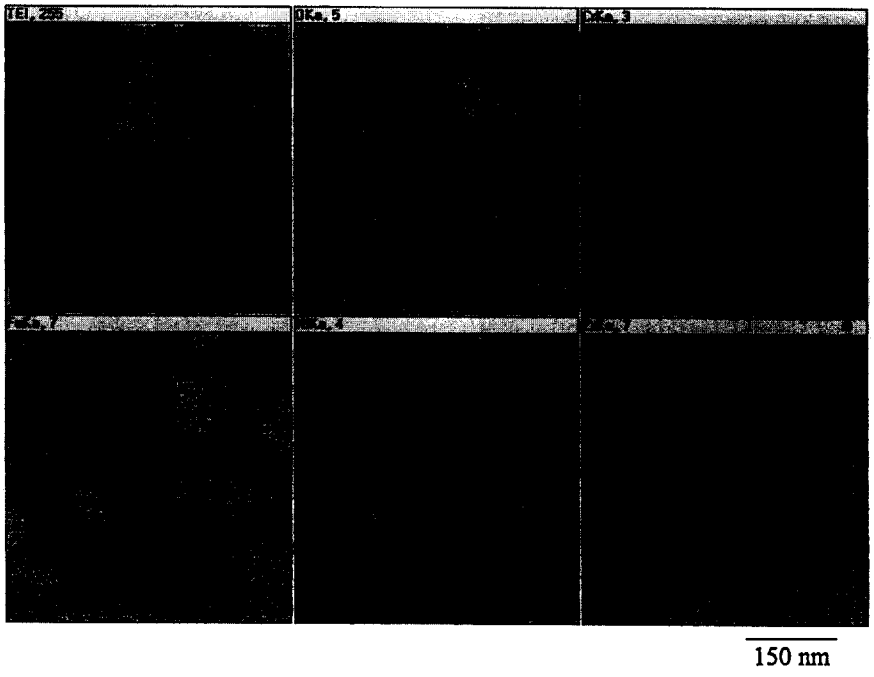

Fig. 17. X-ray maps acquired in STEM mode from the centre of the large precipitate in Fig. 14.

[27,28]. What happens then may depend on the solubility of the Fe^{3+} in ZrO_2. There is some consensus that Fe^{3+} has negligible solubility in m-ZrO_2; up to 5 at.% solubility in t-ZrO_2; and up to 20 at.% in c-ZrO_2, and will stabilise the higher symmetry phases if present at high concentrations [25,26]. This effect on the stability of t-ZrO_2 has

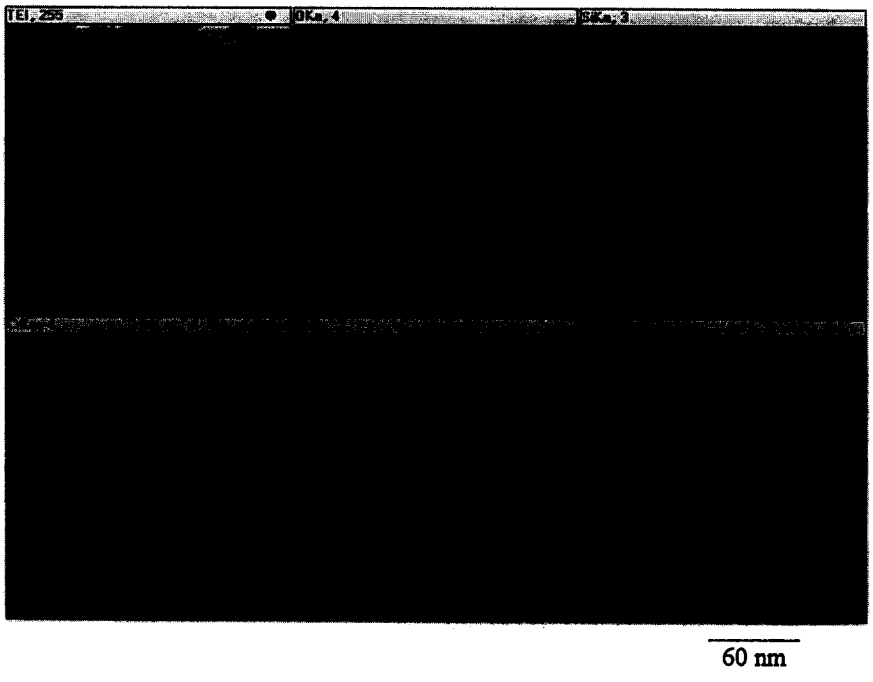

Fig. 18. X-ray maps acquired in STEM mode from an area of oxide formed at 500°C adjacent to an oxidised Zr(Cr, Fe)$_2$ particle, seen at lower right in chromium map in this figure.

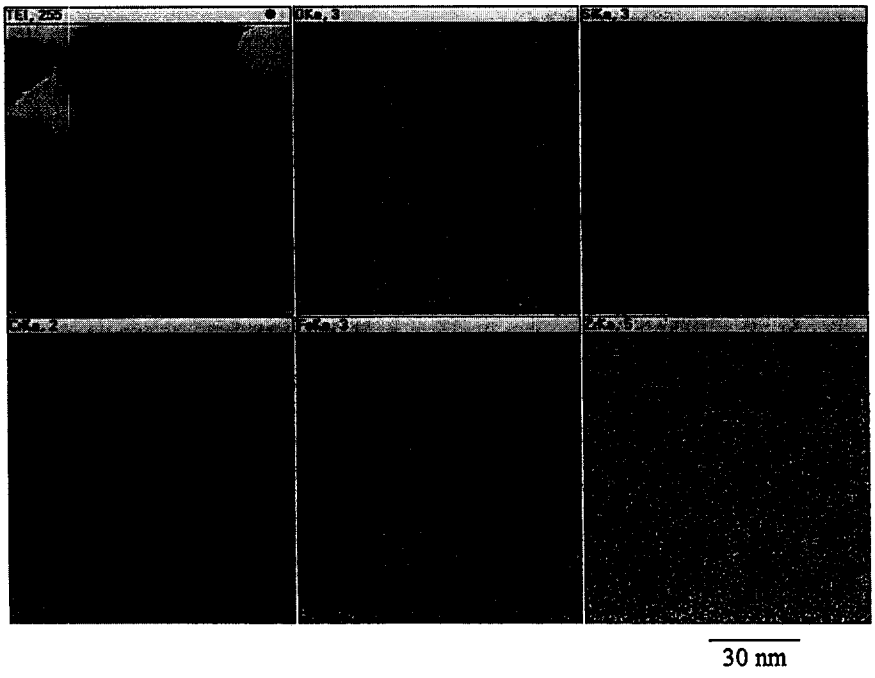

Fig. 19. High-resolution X-ray maps of area at top left of Fig. 18 that showed individual oxide crystallites high in Fe.

already formed the basis of Godlewski's mechanism for the stabilisation of t-ZrO_2 [20].

We may here have an explanation for the formation of discrete high iron crystallites only at some distance from the oxidised intermetallic at 500°C. Close to the particle the oxide may be all t- or c-ZrO_2 [20] and able to accommodate much of the iron from the intermetallic, where it averages about 30 at.%. As it diffuses further from the particle the average Fe concentration will fall below that necessary to stabilise t-ZrO_2, and the Fe can then only be accommodated by forming discrete high Fe crystallites in a surrounding m-ZrO_2 matrix. It is interesting in this context that the maximum Fe content of these high Fe crystallites was about 15 at.% suggesting that they may be c-ZrO_2 [26]. As the iron diffuses further away from the precipitate and the average iron content decreases the numbers of these crystallites should decrease until it is not possible to form them. The migration route may be via the crystallite boundaries because of the low Fe^{3+} concen-

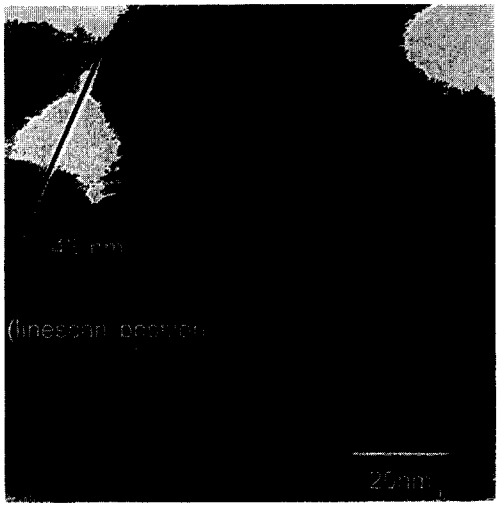

Fig. 20. High-resolution STEM image showing the location of the X-ray linescans acquired from an area of an individual high Fe crystallite that did not show any Moiré fringes.

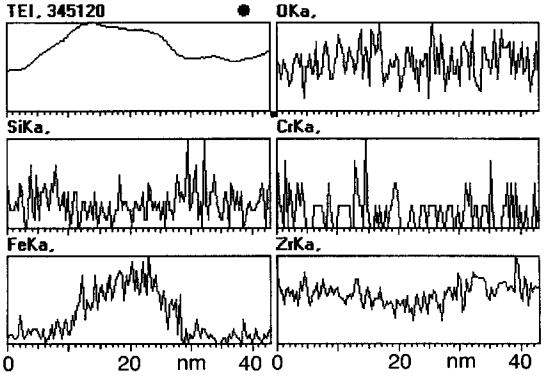

Fig. 21. X-ray line scans acquired from the linescan position shown in Fig. 20.

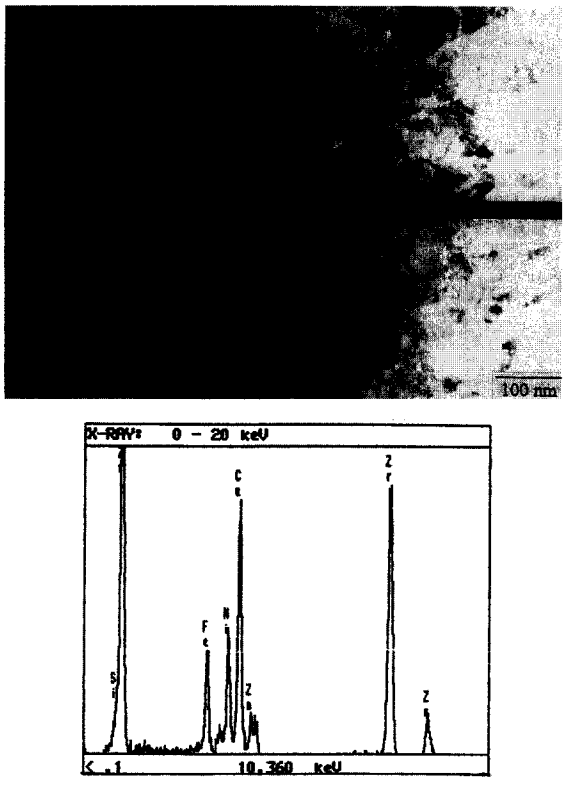

Fig. 22. Zr_2 (Ni, Fe) precipitate (indicated by pointer) oxidized at 600°C and its EDX spectrum.

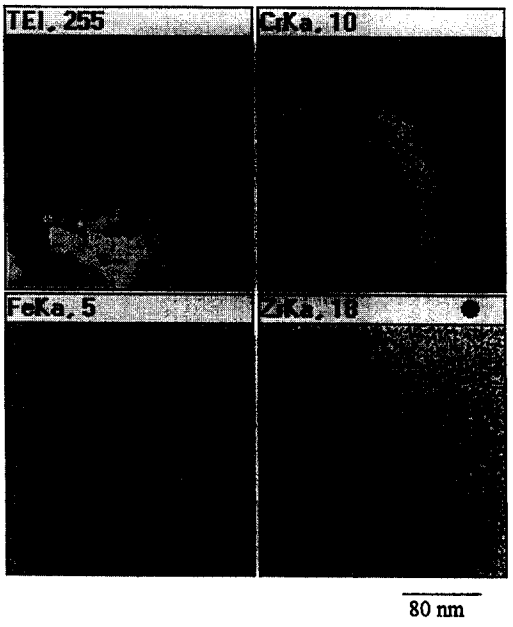

Fig. 24. Total electron image (TEI) and X-ray maps acquired in STEM mode from a $Zr(Cr, Fe)_2$ intermetallic oxidised at 600°C and partially eroded during ion-milling.

tration and solubility in the intervening m-ZrO_2 crystallites, although no evidence for Fe concentration in the boundaries of these crystallites was found. It may be here that the association of Fe and Si aids in the diffusion

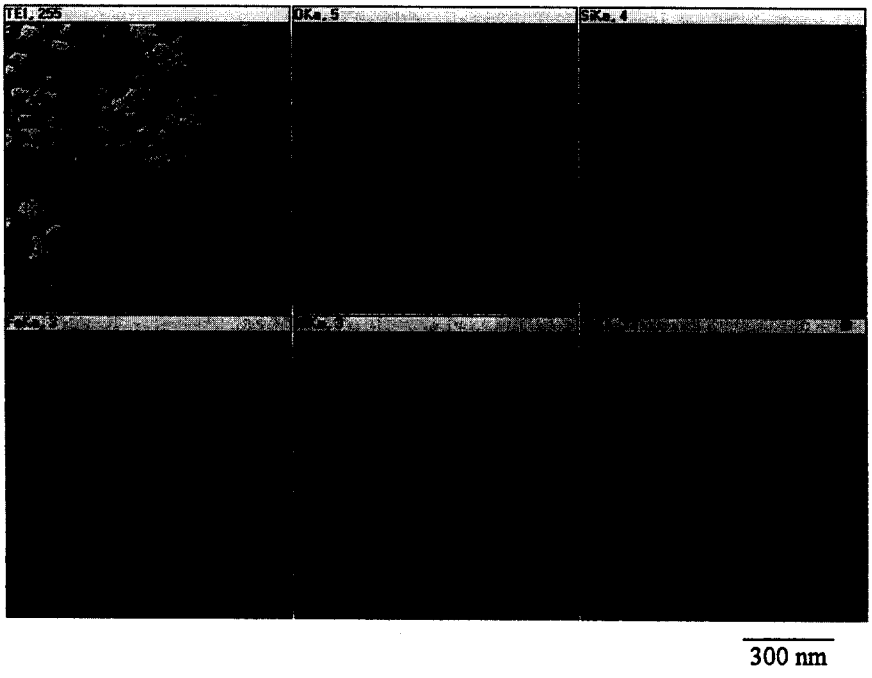

Fig. 23. X-ray maps acquired in STEM mode from the oxidised intermetallic seen in Fig. 22.

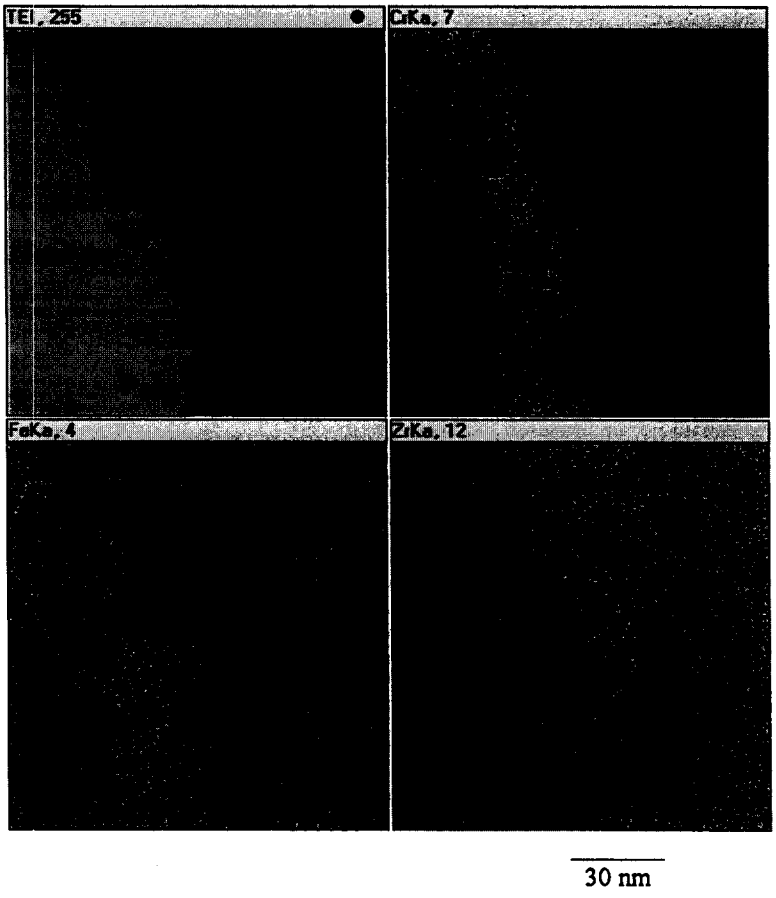

Fig. 25. High-resolution TEI image and X-ray maps acquired from the boundary of the oxidized intermetallic seen in Fig. 24.

process. The intermetallics in this batch of Zircaloy-2 appear to provide a reservoir of Si, since most of the intermetallic particles analysed contained small but measurable amounts of Si.

At and below 400°C the diffusion rates for Fe^{3+} may be too slow to allow such a process, and the iron concentration at the particle boundary too high to form any solid solution in c-ZrO_2, hence the formation of agglomerates of nearly pure iron oxide. The presence of such localised aggregates of iron oxide could be important in the corrosion process in water and lithium hydroxide since they will be much more soluble in these media than the ZrO_2 crystallites. In the thin oxide film region, dissolution of such iron oxide agglomerates could generate pores that would allow water direct access to intermetallic particles while they are still electrically connected to the metal matrix [15]. Under such conditions the cathodic part of the oxidation reaction (the discharge of a proton by an electron) could occur at the intermetallic surface, and easy access of the resulting hydrogen atom to the metal could result. Initial hydrogen uptake rates are known to be very dependent on the chemical composition of the intermetallic phase, and only a very small fraction of the specimen surface has been found to be active at any time [29].

5. Conclusions

High resolution X-ray mapping of oxide sections from Zircaloy-2 specimens oxidised in steam at 400, 500 and 600°C has shown that:

- In the outer part of the oxide, where all the components of the intermetallic particles are oxidised, Fe migrates out of the particle at 400°C to form agglomerates of nearly pure iron oxide around the periphery of the original particle. Cr remains almost entirely within the original particle boundary.
- At 500°C the Fe diffuses further from the original particle and iron oxide agglomerates are not seen. At the limit of the diffusion profile, however, the iron segregates in individual high Fe crystallites that are still primarily ZrO_2. Cr begins to form agglomerates of oxide around the particle periphery at this temperature. The fate of Ni appears to be strongly dependent on the particle size. For

small $Zr_2(Fe/Ni)$ particles migration out of the particle occurs and agglomerates of mixed Fe/Ni oxide are formed; for large ($\geq$ 1 μm) particles these agglomerates remain inside the original particle boundary.

- At 600°C diffusion of Fe and Cr out of the particle into the matrix oxide is much more extensive. Fe is almost uniformly distributed and < 5 at.% remains in the original particle volume. About 15 at.% Cr remains in the original boundary and still preserved a relatively sharp boundary interface.
- Oxide crystallite size within the prior intermetallic boundaries is very small (< 10 nm) and difficult to resolve. At 500°C small crystallites persist in the Fe diffusion zone outside the particle, and a more normal crystallite size (20–40 nm) begins with Fe segregated in individual high Fe crystallites, with Si at their boundaries. At 600°C the large, normal-sized crystallites start at the original particle boundary.
- The migration behaviour of Fe can be explained based on observations in ZrO_2 ceramics, where migration of metallic Fe and association of Fe^{3+} with oxygen vacancies have been observed.

Acknowledgements

The authors are grateful to the Natural Sciences and Engineering Research Council of Canada and the CANDU Owner's Group for the funding that permitted this research to be conducted, and to Fred Pearson, Institute for Materials Research, McMaster University, for assistance on the JEOL-2010F.

References

[1] IAEA-TECDOC-684, Corrosion of Zirconium Alloys in Nuclear Power Reactors, International Atomic Energy Agency, Vienna, 1993.
[2] B. Cox, Intermetallic Particles and Hydrogen Uptake by Zirconium Alloys, Can. Report AECL-9383, 1987.
[3] D. Charquet, E. Alheritiere, in: Proc. Workshop on Second Phase Particles in Zircaloys, Erlangen, KTG, 1985, p. 9.
[4] B. Cox, in: M.G. Fontana, R.W. Staehle, eds., Adv. Corr. Sci. Tech. 5 (1976) 173–391.
[5] K.L. Komarek, M. Silver, in: Proc. Int. Conf. on Thermodynamics of Nuclear Materials, Vienna, International Atomic Energy Agency, 1962, p. 749.
[6] P.J. Shirvington, J. Nucl. Mater. 37 (1970) 177.
[7] R.A. Ploc, B. Cox, in: Proc. Workshop on Second Phase Particles in Zircaloys, Erlangen, KTG, 1985, p. 59.
[8] B. de Gélas, G. Béranger, P. Lacombe, J. Nucl. Mater. 28 (1968) 185.
[9] D. Pêcheur, F. Lefèbvre, A.T. Motta, C. Lemaignan, J.F. Wadier, J. Nucl. Mater. 189 (1992) 318.
[10] H.G. Weidinger, H. Ruhmann, G. Cheliotis, M.A. Maguire, T-L. Yan, in: Proc. 9th Int. Symp. on Zr in the Nuclear Industry ASTM-STP-1132, eds. C.M. Eucken and A.M. Garde (American Society for Testing and Materials, Philadelphia, PA, 1991) p. 499.
[11] B. Cox, Y.-M. Wong, J. Mostaghimi, J. Nucl. Mater. 226 (1995) 272.
[12] B. Cox, Mechanistic Understanding of Nodular Corrosion — The Devil's Advocate's Position, Centre for Nuclear Engineering, Report, CNEUT-94-09, 1994.
[13] Y. Ito, T. Furuya, J. Nucl. Sci. Tech. 32 (1995) 1118.
[14] B. Cox, R.W. Ball, A Study of the Oxide Film Breakdown on Zirconium Alloys by Capacitance Measurements, Canadian Report, AECL-2144, 1964.
[15] B. Cox, M. Ungurelu, Y-M. Wong, C. Wu, in: Proc. 11th Int. Symp. on Zr in the Nuclear Industry, ASTM-STP-1295, eds. E.R. Bradley and G.P. Sabol (American Society for Testing and Materials, W. Conshohocken, PA, 1996) p. 114.
[16] S.B. Newcomb, C.B. Boothroyd, W.M. Stobbs, J. Microsc. 40 (1985) 195.
[17] G.P. Airey, G.P. Sabol, J. Nucl. Mater. 45 (1972/73) 60.
[18] H-J. Beie, A. Mitwalsky, F. Garzarolli, H. Ruhmann, H-J. Sell, in: Proc. 10th Int. Symp. on Zr in the Nuclear Industry, ASTM-STP-1245, eds. A.M. Garde and E.R. Bradley (American Society for Testing and Materials, Philadelphia, PA, 1994) p. 615.
[19] T. Kubo, M. Uno, in: C.M. Eucken and A.M. Garde, eds., Proc. 9th Int. Symp. on Zr in the Nuclear Industry, ASTM-STP-1132 (American Society for Testing and Materials, Philadelphia, PA, 1991) p. 476.
[20] J. Godlewski, in: Proc. 10th Int. Symp. on Zr in the Nuclear Industry, ASTM-STP-1245, eds. A.M. Garde and E.R. Bradley (American Society for Testing and Materials, Philadelphia, PA, 1994) p. 663.
[21] D. Pêcheur, F. Lefèbvre, A.T. Motta, C. Lemaignan, D. Charquet, in: Proc. 10th Int. Symp. on Zr in the Nuclear Industry, ASTM-STP-1245, eds. A.M. Garde and E.R. Bradley (American Society for Testing and Materials, Philadelphia, PA, 1994) p. 687.
[22] K. Kajihara, Y. Yoshizawa, T. Sakuma, Acta Metall. Mater. 43 (1995) 1235.
[23] K. Nakashima, K. Takihara, T. Miyazaki, K. Mori, J. Am. Ceram. Soc. 76 (1993) 3000.
[24] P. Li, I.W. Chen, J. Am. Ceram. Soc. 77 (1994) 118.
[25] S. Davison, R. Kershaw, K. Dwight, A. Wold, J. Solid State Chem. 73 (1988) 47.
[26] J.N. Karavaev, S.F. Palguev, A.D. Neujmin, in: High Tech. Ceramics, ed. P. Vincenzini (Elsevier, Amsterdam, 1987) p. 247.
[27] H.A. Porte, J.G. Schnizlein, R.C. Vogel, D.F. Fischer, J. Electrochem. Soc. 107 (1960) 506.
[28] R.D. Misch, C. van Drunen, Proc. USAEC Symp. on Zr Alloy Development, Castlewood, CA, Nov. 1962, US Report GEAP-4089, Vol. II, pap. 15.
[29] B. Cox, J. Alloys Comp., to be published.